



Contents lists available at ScienceDirect

Journal of the Mechanics and Physics of Solids

journal homepage: www.elsevier.com/locate/jmps

Nutations in growing plant shoots: The role of elastic deformations due to gravity loading

Daniele Agostinelli^a, Alessandro Lucantonio^b, Giovanni Noselli^a,
Antonio DeSimone^{a,b,*}

^aSISSA–International School for Advanced Studies, Trieste 34136, Italy

^bThe BioRobotics Institute, Scuola Superiore Sant'Anna, Pisa 56127, Italy

ARTICLE INFO

Article history:

Received 1 July 2019

Revised 24 August 2019

Accepted 25 August 2019

Available online xxx

Keywords:

Circumnutations

Gravitropism

Hopf bifurcation

Flutter instability

ABSTRACT

The effect of elastic deformations induced by gravity loading on the active circumnutation movements of growing plant shoots is investigated. We consider first a discrete model (a gravitropic spring-pendulum system) and then a continuous rod model which is analyzed both analytically (under the assumption of small deformations) and numerically (in the large deformation regime). We find that, for a choice of material parameters consistent with values reported in the available literature on plant shoots, rods of sufficient length may exhibit lateral oscillations of increasing amplitude, which eventually converge to limit cycles. This behavior strongly suggests the occurrence of a Hopf bifurcation, just as for the gravitropic spring-pendulum system, for which this result is rigorously established. At least in this restricted set of material parameters, our analysis supports a view of Darwin's circumnutations as a biological analogue to structural systems exhibiting flutter instabilities, *i.e.*, spontaneous oscillations away from equilibrium configurations driven by non-conservative loads. Here, in the context of nutation movements of growing plant shoots, the energy needed to sustain oscillations is continuously supplied to the system by the internal biochemical machinery presiding the capability of plants to maintain a vertical pose.

© 2019 The Authors. Published by Elsevier Ltd.

This is an open access article under the CC BY-NC-ND license.

(<http://creativecommons.org/licenses/by-nc-nd/4.0/>)

1. Introduction

Nutations and circumnutations, namely, periodic movements in rapidly elongating plant organs such as roots, hypocotyls, shoots, branches, and flower stalks have fascinated scientists for over a century. A large body of literature has followed the seminal work by Darwin (1880), see Schuster (1996) and Mugnai et al. (2015) for a (partial) list of references. In one of the prevailing theories currently accepted, nutations are oscillatory movements arising from the over-compensatory response of a plant to the changing orientation of its gravisensory apparatus relative to the Earth's gravity vector. Contributions of particular relevance are Israelsson and Johnsson (1967), Johnsson and Heathcote (1973) and Johnsson et al. (2009). Very recently, quantitative models supporting this hypothesis have been proposed and tested, see *e.g.*, Bastien et al. (2013),

* Corresponding author at: SISSA–International School for Advanced Studies, Via Bonomea 265, Trieste 34136, Italy.

E-mail addresses: daniele.agostinelli@sissa.it (D. Agostinelli), alessandro.lucantonio@santannapisa.it (A. Lucantonio), giovanni.noselli@sissa.it (G. Noselli), desimone@sissa.it (A. DeSimone).

<https://doi.org/10.1016/j.jmps.2019.103702>

0022-5096/© 2019 The Authors. Published by Elsevier Ltd. This is an open access article under the CC BY-NC-ND license.

(<http://creativecommons.org/licenses/by-nc-nd/4.0/>)

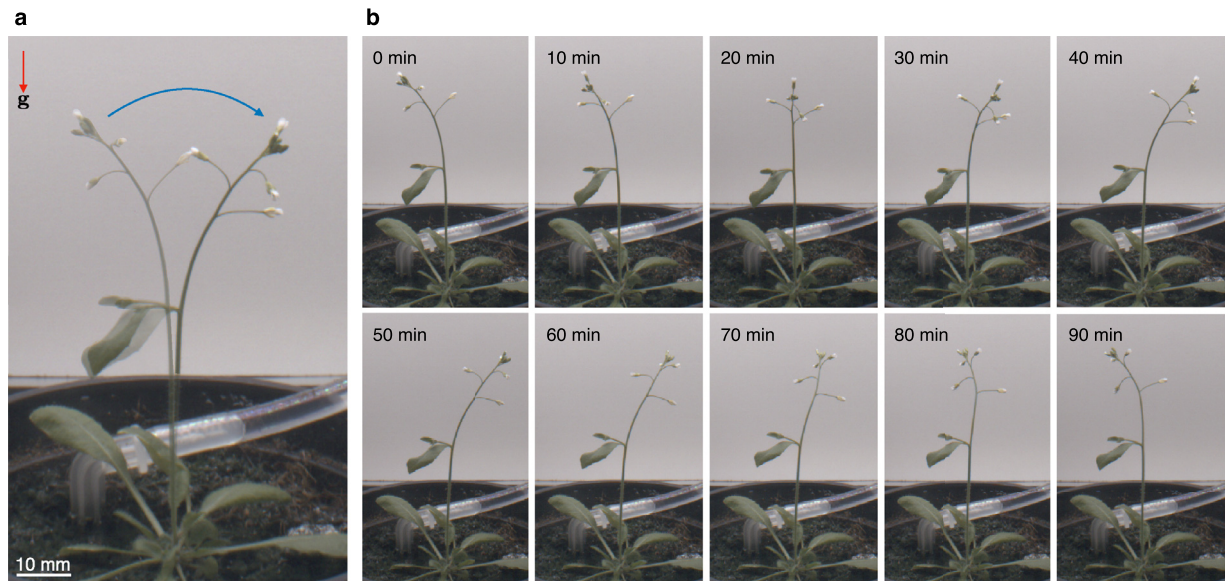


Fig. 1. A 40-day-old sample of *Arabidopsis thaliana* (ecotype Col-0) grown under normal gravity conditions (1 g) at the SAMBA laboratory of SISSA. (a) A superposition of two snapshots to highlight the amplitude of lateral oscillations (circumnutations) exhibited by the primary shoot. (b) A sequence of snapshots taken at time intervals of 10 minutes. Notice that the characteristic time of circumnutational oscillations is of the order of $\tau_c \approx 90$ min.

Bastien et al. (2014), Chelakkot and Mahadevan (2017), Pouliquen et al. (2017) and Meroz et al. (2019) and the microscopic mechanisms governing gravisensing have been identified (Chauvet et al., 2019).

In this paper, building on the observation that growing shoots often appear as elongated biological structures of significant weight relative to their stiffness, we focus on the role that elastic deformations arising from gravity loading may have on the nutational movements. We analyze these movements as a Hopf bifurcation phenomenon in the equations governing the gravitropic dynamics of a growing shoot, and identify the regime of material and geometric parameters in which this bifurcation, and hence nutation movements, are likely to occur. As discussed in the manuscript, the parameters which come into play are four characteristic times, namely, the duration of statoliths avalanche in the statocytes τ_a , the growth time τ_g , the memory time τ_m , the reaction time τ_r , and two dimensionless loading parameters, that is, γ and λ , determined by the shoot weight and slenderness, respectively.

Typically, elastic deformations are just one of the concurrent factors promoting oscillatory response. There are however regimes of the governing parameters, identified by values of the four characteristic response times and of the two dimensionless loading parameters, in which taking into account the elastic deformations induced by gravity loading is necessary to “explain” the emergence of oscillations. At least in this restricted set of geometric and material parameters, our analysis supports a view of Darwin’s circumnutations as a biological analogue to structural systems exhibiting flutter instabilities, *i.e.*, spontaneous oscillations away from equilibrium configurations. In recent papers appeared in this journal, these have been analyzed in structural systems loaded by non-conservative (follower) forces, see Bigoni and Noselli (2011) and Bigoni et al. (2018). Here, in the context of nutation movements of growing plant shoots, the energy needed to sustain oscillations is continuously supplied to the system by the internal biochemical machinery presiding the capability of plants to maintain a vertical pose.

1.1. State of the art: a brief review

Movements of growing plant organs are very complex and far from being completely understood. The observable shape of a plant is the specific result of its unique history of endogenous and exogenous factors. Discerning whether certain dynamics are encoded in the biology of the system or they represent the mechanical and physiological reaction to external cues, or a combination of both, is a fundamental question that has intrigued and puzzled many scientists over the past two centuries.

Movements in plants are mainly classified in tropisms and nastic movements. Tropisms are the directed growth responses to directional environmental cues, *e.g.*, light (*phototropism*), gravity (*gravitropism*), touch (*thigmotropism*), etc, while nastic movements are motions responding to external stimuli which are independent of the position of the stimulus source, *e.g.*, temperature (*thermonasty*), chemicals (*chemonasty*), touch (*thigmonasty*), etc.

This classification fails to include circumnutational movements, *i.e.*, circular, elliptical or pendular oscillations of elongating plant organs (exemplified in Fig. 1 for *Arabidopsis thaliana* Col-0), which are caused by radially asymmetric growth rates that have uncertain origin. The first reports about circumnutations can be traced back to the 19th century and, since then, many different terms have been used in the literature to refer to such a phenomenon. Indeed, Palm (1827) talked about

twining, von Sachs (1875) used the term *revolving nutation*, Darwin (1880) coined the term *circumnutation*, Noll (1885) reported about *rotating nutations*, Gradmann (1922) about *over-bending movements*, Rawitscher (1932) about *circular movements*, Bünning (1953) about *circumnasty* and Hammer and Gessner (1958) about *growth oscillations*.

It seems widely accepted that circumnutations are the consequence of helical growth and reversible cell volume variations (Mugnai et al., 2015). However, consensus on the regulatory mechanism of circumnutations has not been reached yet, with opinions split between two main theories: circumnutations can be explained either by endogenous mechanisms or as internal responses to exogenous stimuli. In the first case, circumnutations should constitute a class of movements on their own (Correll and Kiss, 2008), whereas in the second case, they should be included among tropisms or nastic movements.

Darwin (1880) was probably the first one to suggest an endogenous feature of circumnutations whose “amplitude, or direction, or both have only to be modified for the good of the plant in relation with internal or external stimuli”. Theories supporting this point of view included hormonal and ionic oscillations with gravity acting as an external signal. Arnal (1953) proposed periodic variations in auxin fluxes from the tip and Joerrens (1957) hypothesized periodic changes in the sensitivity of the elongating cells to auxin. Heathcote and Aston (1970) formulated the theory of a nutational oscillator situated in each cell. Studying shoots in *Phaseolus Vulgaris* L., Millet et al. (1984), Millet et al. (1988) and Badot et al. (1990) proposed a primary mechanism residing in the moving of a turgescence wave around the shoot, also related to K distribution. More recently, Shabala and Newman (1997) and Shabala (2003) observed strong correlations between nutation and rhythmical patterns of H^+ , K^+ and Ca^{2+} ion fluxes in the elongation region of corn roots.

On the other side, Gradmann (1926) introduced the idea that circumnutations could be the result of delayed gravitropic responses: the deviation from the vertical line triggers a correcting movement that, due to a reaction time between perception and actuation, makes the plant overshoot giving rise to self-sustained oscillations. Building on this, Israelsson and Johnsson (1967) and Somolinos (1978) showed that a model describing the plant gravitropic response based on delay and memory could explain circumnutations. Later, observing an autotropic straightening to a vertical position in *Avena* seedlings during weightlessness experiments, Chapman et al. (1994) adapted the model proposed by Israelsson and Johnsson (1967) by including such autotropic effects.

The debate about the role of gravity for the induction or continuation of circumnutations persisted and has been fueled by new experiments on Earth and in space over the last few decades (Kiss, 2006; 2009; Kobayashi et al., 2019). On the one hand, the study of agravitropic mutants in morning glory, pea and arabidopsis supported the idea that gravireponse is required in both the shoots and roots of dicotyledonous plants (Hatakeda et al., 2003; Kim et al., 2016; Kitazawa et al., 2005; 2008). On the other hand, many experimental results have been interpreted as corroborating the Darwinian theory of endogenous oscillations affected by graviresponses. Based on experiments in microgravity reported by Brown and Chapman (1984), Brown et al. (1990) and Johnsson et al. (1999) suggested a two-oscillator model by combining the gravitropic feedback oscillator with an endogenous oscillator. Performing experiments on the gravitropic rice mutant *lazy1*, Yoshihara and Iino (2006) concluded that circumnutation and gravitropism are separate (although interfering) phenomena. Moreover, “minute oscillatory movements in microgravity” have been observed by Johnsson et al. (2009) in *A. thaliana* and, more recently, also Kobayashi et al. (2019) reported minute movements in rice coleoptiles in microgravity, although cautiously stressing the fact that such movements were difficult to measure and it was “technically difficult to determine whether they were truly circumnutation or not”.

In addition, another important unsolved issue is to which extent the role of gravity depends on the plant organs or species. For instance, tillers of the rice mutant *lazy1* behave differently from coleoptiles (Abe et al., 1996), and evolutionary benefits are obvious for twining plants in search of mechanical support. In any case, it is clear that considerable deviations from the plumb line will cause a gravitropic reaction, possibly interfering with an endogenous oscillator (assuming this oscillator exists). This is the reason why gravitropism plays a crucial role when dealing with circumnutations. In general, the study of any kind of tropism consists in understanding the mechanisms of stimulus perception, signal transduction and response.

The concept of tropism was introduced by Knight in 1806 but only recently “the data converged to provide a picture of the physiological, molecular and cell biological processes that underlie plant tropisms” (Gilroy and Masson, 2008). About gravitropism, it is widely accepted that plants sense gravity in specialized cells (statocytes) through the sedimentation of starch-filled plastids (statoliths) which are denser than the surrounding cellular fluid. This leads to the development of an asymmetry in auxin concentration between the upper and lower flanks, causing differential cell elongation and hence bending.

The standard way to model gravitropism goes back to Von Sachs (1882), who formulated the so-called *sine law* stating that the gravireponse is proportional to the sine of the angle formed by the vertical and the organ axis. An important modification to the sine law has been introduced by Bastien et al. (2013) and Bastien et al. (2014), who included a proprioception term to describe the phenomenon of organ straightening called autotropism. However, in the last few decades, an apparent contradiction emerged when testing this law: under permanent inclination, the response of the plant appeared to be independent of effective gravity, whereas, under transient gravi-stimulation, the gravireponse was quantified by a *dose-response* curve, the dose depending on the stimulation time and the effective gravity (Chauvet et al., 2019). By introducing a memory process in the gravitropic signalling pathway (using an approach already proposed by Israelsson and Johnsson (1967) and similarly taken by Meroz et al. (2019)) and a microscopic description of the statoliths dynamics, Chauvet et al. (2019) identified four time-scales regulating the gravireponse. In this unified framework, the gravity-independent sine law is recovered when the stimulation is long enough compared to the statolith avalanche duration and the memory time, while dose-

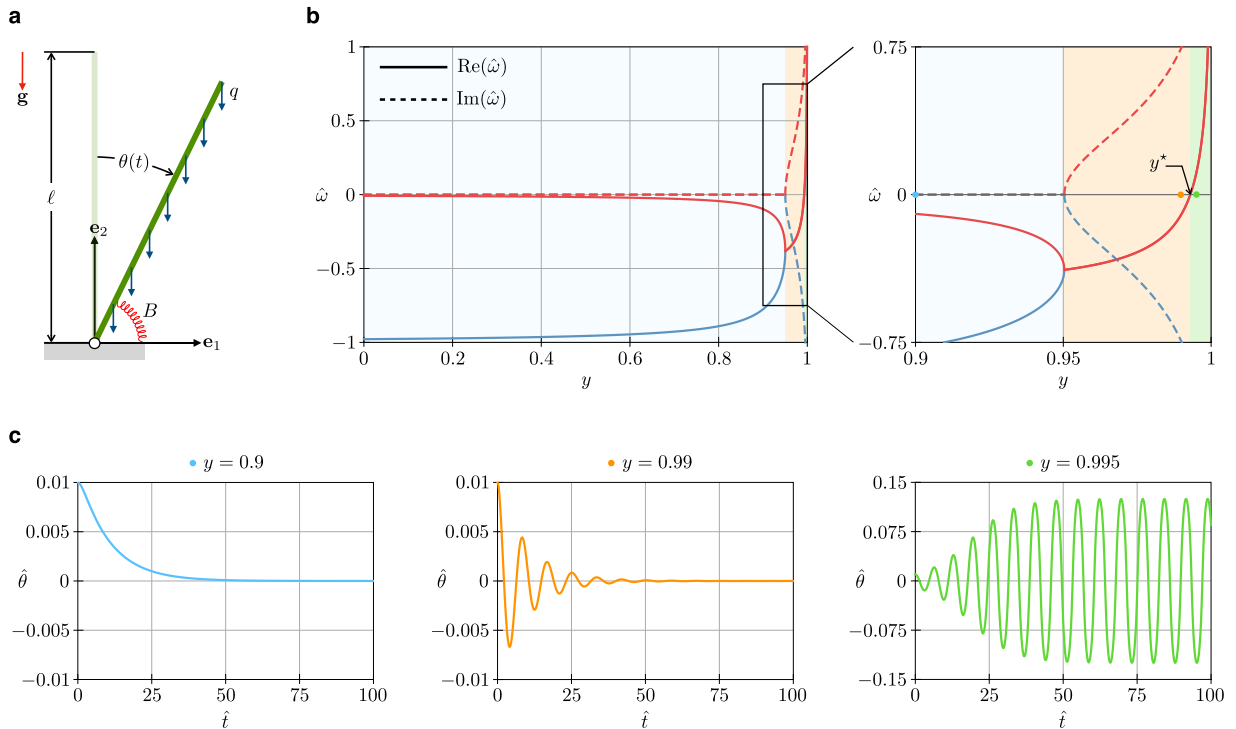


Fig. 2. (a) A sketch of the one-degree-of-freedom gravitropic spring-pendulum system discussed in the manuscript. (b) Real (solid lines) and imaginary (dashed lines) part of the roots of the characteristic equation (11) as functions of $y \in [0, 1]$ for $\eta = 1$ and $\sigma = 0.008$. We distinguish three regions corresponding to three distinct behaviours of the fixed point $\hat{\theta} = 0$: (i) a stable node (light blue), (ii) a stable spiral (orange), and (iii) an unstable spiral converging to a stable limit cycle (green). (c) Numerical solutions of the nonlinear discrete delay differential Eq. (6) at increasing values of the parameter y and for $\hat{\theta}(\hat{t}) = 0.01$ for $\hat{t} \leq 0$. Specifically, the angular coordinate $\hat{\theta}$ is reported as a function of dimensionless time \hat{t} for $y = 0.9$ (light blue curve), $y = 0.99$ (orange curve), and $y = 0.995$ (green curve). (For interpretation of the references to colour in this figure legend, the reader is referred to the web version of this article.)

responses are obtained either when the time of the stimulation is shorter than the avalanche time or when it is longer than that but shorter than the memory time.

In this scenario, elastic deformations due to gravity loading have been often overlooked. Here, we have made an effort to take them into account building on the recent advances in the understanding of gravitropic and autotropic responses (Chauvet et al., 2019; Dumais, 2013; Hamant and Mouliia, 2016) and in the modeling of the additional effects due to elastic deflections through the separation of sensed and actuated variables (Chelakkot and Mahadevan, 2017).

2. A gravitropic spring-pendulum system

We begin our study on circumnutations of growing shoots by exploring the dynamics of a prototypical system consisting of an upward vertical pendulum supported by a “gravitropic” torsional spring which adapts its rest angle to reorient the pendulum in the direction opposite to gravity.

Specifically, let us consider a rigid bar of length ℓ , hinged at the bottom and supported by a spring of torsional stiffness $B > 0$, see Fig. 2a. The bar carries its weight, modelled by a vertical distributed load of magnitude q , and is confined to the plane $\{\mathbf{e}_1, \mathbf{e}_2\}$ so that its configuration is determined at any time t by the angle $\theta(t)$ with respect to the vertical.

Equilibrium of the pendulum under the prescribed distributed load requires that

$$m(\theta, \theta_0) = \frac{1}{2} q \ell^2 \sin \theta, \tag{1}$$

where $m(\theta, \theta_0)$ is the torque exerted by the spring. As for its constitutive characterization, we consider the affine law

$$m(\theta, \theta_0) = B(\theta - \theta_0), \tag{2}$$

where θ_0 is the time-dependent rest angle for which we assume the following time evolution law

$$\dot{\theta}_0(t) = -\frac{\beta}{\tau_g \tau_m} \int_{-\infty}^{t-\tau_r} e^{-\frac{1}{\tau_m}(t-\tau_r-\tau)} \sin \theta(\tau) d\tau, \tag{3}$$

where a dot denotes differentiation with respect to time. In the equation above, $\beta \geq 0$ is the dimensionless gravitropic sensitivity, $\tau_g > 0$ is the characteristic time for the evolution of the rest angle, $\tau_r \geq 0$ is the geotropic reaction time or delay,

whereas $\tau_m > 0$ is a parameter of the exponential weighting function defining the plant's memory of the stimulus. The evolution law (3) was initially proposed by Israelsson and Johnsson (1967) to model the response of growing plants to gravi-stimulation. This has been recently improved by Chauvet et al. (2019) to account for the dynamics of statoliths sedimentation, as discussed in the manuscript.

For the special case of $\beta = 0$ the time evolution of the rest angle is inhibited. It follows that $\theta_0(t) \equiv 0$, such that the vertical configuration is an equilibrium which loses stability as the length of the pendulum exceeds a critical value ℓ_c (buckling critical length). This can easily be computed through a stability analysis of the spring-pendulum system, leading to

$$\ell_c := \sqrt{\frac{2B}{q}}. \tag{4}$$

Our goal is to consider the more general case of $\beta \neq 0$ and to explore the behaviour of the spring-pendulum system as its length increases. We anticipate that our analysis will reveal that the trivial equilibrium $(\theta, \theta_0) = (0, 0)$ undergoes a supercritical Hopf bifurcation at a pendulum length of the order of ℓ_c . To that aim, we proceed by taking the derivative of the balance Eq. (1). Substitution of (3) leads to

$$\dot{\theta}(t) \left(1 - \frac{q \ell^2}{2B} \cos \theta(t) \right) = - \frac{\beta}{\tau_g \tau_m} \int_{-\infty}^{t-\tau_r} e^{-\frac{1}{\tau_m}(t-\tau_r-\tau)} \sin \theta(\tau) \, d\tau, \tag{5}$$

such that by a further differentiation with respect to time we arrive at

$$\left(1 - \frac{q \ell^2}{2B} \cos \theta(t) \right) \left(\ddot{\theta}(t) + \frac{1}{\tau_m} \dot{\theta}(t) \right) + \frac{q \ell^2}{2B} \dot{\theta}^2(t) \sin \theta(t) + \frac{\beta}{\tau_g \tau_m} \sin \theta(t - \tau_r) = 0. \tag{6}$$

We notice that, in the absence of external loading ($q = 0$), (6) reduces to the so-called "sunflower" equation. This model was proposed by Israelsson and Johnsson (1967) to interpret the geotropic circumnutations of the apical region of plants, and has already been proved to admit periodic solutions (Somolinos, 1978) for a specific range of parameters. However, growing shoots often appear as elongated, biological structures of significant weight relative to their stiffness, a fact that cannot be disregarded. This is evident from the parameter $q \ell^2 / (2B)$ in the equation above, measuring the relative magnitude of the plant's weight to stiffness.

To explore the effect of elastic deformations of the pendulum due to gravity loading, we proceed by linearizing Eq. (6) about $\theta = 0$ to derive the following second order discrete delay differential equation

$$\left(1 - \frac{q \ell^2}{2B} \right) \left(\ddot{\theta}(t) + \frac{1}{\tau_m} \dot{\theta}(t) \right) + \frac{\beta}{\tau_g \tau_m} \theta(t - \tau_r) = 0, \tag{7}$$

which, assuming $\tau_r > 0$, can be restated in dimensionless form upon introduction of three dimensionless parameters, i.e.,

$$y := \frac{q \ell^2}{2B}, \quad \eta := \frac{\tau_r}{\tau_m}, \quad \sigma := \beta \frac{\tau_r^2}{\tau_g \tau_m}, \tag{8}$$

leading to

$$(1 - y) \left(\ddot{\hat{\theta}}(\hat{t}) + \eta \dot{\hat{\theta}}(\hat{t}) \right) + \sigma \hat{\theta}(\hat{t} - 1) = 0, \tag{9}$$

where $\hat{\theta}(\hat{t}) := \theta(\hat{t} \tau_r)$ and a superimposed dot denotes now differentiation with respect to the dimensionless time $\hat{t} := t / \tau_r$.

Here, we prefer to omit the details of our analysis to focus instead on the following, important result. In fact, application of the theorems reported in Appendix A leads to the conclusion that (9) exhibits a supercritical Hopf bifurcation at

$$y = y^* := 1 - \frac{\sigma \sin \xi^*}{\eta \xi^*}, \tag{10}$$

where ξ^* is defined as the unique root of $\xi = \eta \cot \xi$ in $(0, \pi/2)$. Notice that $y = (\ell / \ell_c)^2$, such that we propose the following physical interpretation of the result above: in a growing shoot subject to gravity, circumnutations may arise as a consequence of a Hopf bifurcation as the shoot's length attains the critical value $\ell^* := \sqrt{y^*} \ell_c$. We infer from Eq. (10) that $y^* < 1$, so that $\ell^* < \ell_c$, i.e., the delayed graviresponse triggers a Hopf bifurcation before the buckling critical length is reached. This conclusion is further supported by the analysis of the roots of the characteristic equation relative to (9)

$$(1 - y) (\hat{\omega}^2 + \eta \hat{\omega}) e^{\hat{\omega}} + \sigma = 0, \tag{11}$$

obtained by plugging in it the representation $\hat{\theta}(\hat{t}) = e^{\hat{\omega} \hat{t}}$ for the angular coordinate, where $\hat{\omega}$ is a dimensionless circular frequency. We report in Fig. 2b the real (solid lines) and the imaginary (dashed lines) part of the roots of the characteristic Eq. (11) as functions of the loading parameter $y \in [0, 1]$ for $\eta = 1$ and $\sigma = 0.008$. These values were determined by assuming a gravitropic sensitivity of $\beta = 0.8$, $\tau_g = 1200$ min, and $\tau_r = \tau_m = 12$ min, see Chauvet et al. (2019), and correspond to a critical loading parameter of $y^* \approx 0.993$.

In the figure, we distinguish three regions corresponding to distinct behaviours of the fixed point $\hat{\theta} \equiv 0$: (i) a stable node (light blue region, where roots are real and negative), (ii) a stable spiral (orange region, where roots are complex conjugate

with negative real part), and (iii) an unstable spiral converging to a stable limit cycle (green region, where roots are complex conjugate with positive real part) for $y > y^*$. The figure also reports numerical solutions of the nonlinear discrete delay differential Eq. (6) at increasing values of the parameter y and for the initial condition of $\hat{\theta}(\hat{t}) = 0.01$ for $\hat{t} \leq 0$. Specifically, Fig. 2c shows the angular coordinate $\hat{\theta}$ as a function of dimensionless time \hat{t} for $y = 0.9$ (light blue curve), $y = 0.99$ (orange curve), and $y = 0.995$ (green curve). The numerical implementation of the nonlinear Eq. (6) was achieved by exploiting the NDSolve functionality of Mathematica v11.3.0.0 and confirms the onset of periodic solutions in correspondence with the theoretical Hopf bifurcation point.

We notice, in passing, that the distributed delay of (5) is not necessary to give rise to such a qualitative behaviour. Indeed, the following first order differential equation with discrete delay

$$\dot{\theta}(t)(1 - y \cos \theta(t)) = -\frac{\beta}{\tau_g} \sin \theta(t - \tau_r) \quad (12)$$

has the same qualitative features and undergoes a supercritical Hopf bifurcation at

$$y_0^* := 1 - \frac{2}{\pi} \frac{\sigma}{\eta}. \quad (13)$$

Eq. (12) can be recovered from Eq. (5) by letting $\tau_m \searrow 0$ (as the gravitropic memory kernel in (5) tends to a Dirac delta in the sense of distributions) and, consistently, $y^* \nearrow y_0^*$.

In concluding this section, we find it useful to stress the significance of elastic deformations due to gravity in determining the oscillatory behaviour sometimes exhibited by growing shoots. In fact, by neglecting the effect of either external loading ($q \rightarrow 0$) or of elastic deformations ($B \rightarrow \infty$), one would constrain the parameter y to null, such that self-sustained oscillations would be impossible, at least for the chosen values of the parameters, which are the most realistic ones to characterize the biological machinery regulating the gravitropic response of plant organs.

3. A rod model for growing shoots

Inspired by the prototypical system studied in Section 2, we introduce a planar rod model that accounts for growth by cell expansion and for the evolution of spontaneous curvature due to gravitropism and proprioception. For the evolution laws that govern the active response of the rod we rely on recent developments from the available literature. Finally, we derive a reduced model that is appropriate for the study of circumnutations in young plant shoots.

3.1. Mechanics

We model the plant shoot as an unshearable and (elastically) inextensible rod confined to the plane spanned by $\{\mathbf{e}_1, \mathbf{e}_2\}$. At each time t its centreline $\mathbf{r}(s, t)$ is a planar C^2 curve of length $\ell(t)$ parametrized by the arc-length $s \in [0, \ell(t)]$. The rod undergoes an extensional growth characterized by a prescribed time evolution of the actual stretch

$$\lambda(S_0, t) = \frac{\partial s}{\partial S_0}(S_0, t), \quad (14)$$

where $S_0 \in [0, \ell(0)]$ is the reference arc-length, and $s(S_0, t)$ denotes the change of coordinate in C^1 that at any time t maps S_0 into the current arc-length.

We denote by $\theta(s, t)$ in C^2 the angle between the unit vector \mathbf{e}_2 pointing in the vertical direction and the local tangent to the curve, see Fig. 3a. Then, the unit tangent to the rod axis is

$$\mathbf{r}' = \sin \theta \mathbf{e}_1 + \cos \theta \mathbf{e}_2, \quad (15)$$

where a prime denotes differentiation with respect to s , such that the configuration of the rod can be reconstructed from θ as

$$\mathbf{r}(s, t) = \mathbf{r}_0 + \int_0^s \mathbf{r}'(\sigma, t) d\sigma, \quad (16)$$

where \mathbf{r}_0 is the position of the basal end.

Since we have in mind processes where the time-scale for mechanical equilibrium is much shorter than any biological time-scale of the plant, we impose static equilibrium at any time, i.e.,

$$\mathbf{n}' + \mathbf{f} = \mathbf{0}, \quad \mathbf{m}' + \mathbf{r}' \times \mathbf{n} = \mathbf{0}, \quad (17)$$

where \mathbf{n} and \mathbf{m} are the resultant contact force and contact couple, whereas \mathbf{f} is the body force per unit current length. From the planarity assumption, $\mathbf{n} = n_1 \mathbf{e}_1 + n_2 \mathbf{e}_2$ and $\mathbf{m} = m_3 \mathbf{e}_3$ and, from the physics of the problem, we prescribe $\mathbf{f} = -q\mathbf{e}_2$ where q denotes the plant's weight per unit current length.

As for the constitutive response of the rod to bending, we follow the approach by Chelakkot and Mahadevan (2017) and assume a linear Euler-Bernoulli law such that

$$m_3(s, t) = -B(s, t)[\theta'(s, t) - \kappa(s, t)], \quad (18)$$

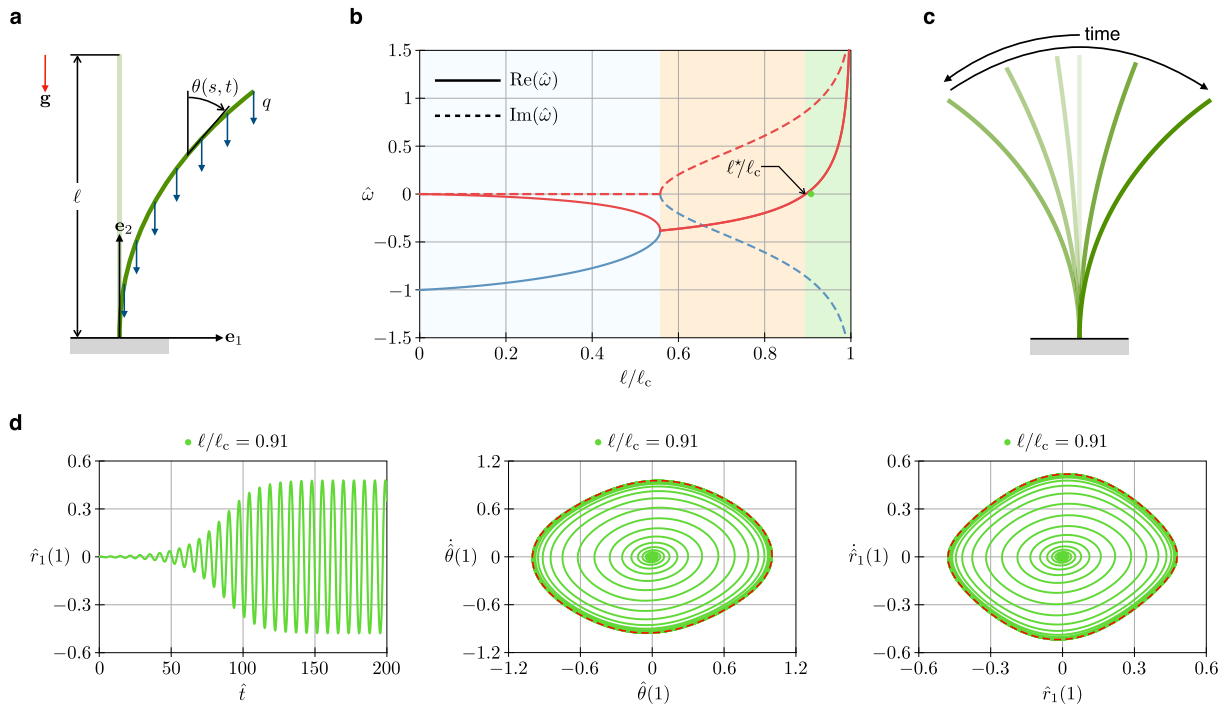


Fig. 3. (a) A sketch of the planar rod model for the analysis of periodic oscillations in plant shoots. (b) Real (solid lines) and imaginary (dashed lines) part of the roots of the characteristic Eq. (37) as functions of $\ell/\ell_c \in [0, 1]$ and for the choice of parameters introduced in Section 4.1. As for the case of the gravitropic spring-pendulum system, we distinguish three regions corresponding to different dynamical responses for $\hat{\theta}(\xi, \hat{t})$: (i) an exponential decay (light blue), (ii) a damped oscillation (orange), and (iii) an increasing oscillation (green) for $\ell > \ell^* \approx 0.895 \ell_c$. (c) Superimposition of deformed shapes from the nonlinear rod model as computed for $\ell = 0.91 \ell_c$ as the time spans half a period of the limit cycle. (d) Numerical solutions of the nonlinear problem (24)–(26) as obtained for $\ell = 0.91 \ell_c$. Specifically, the transverse displacement and the phase portraits related to the angle and position of the rod's tip as functions of time are shown. (For interpretation of the references to colour in this figure legend, the reader is referred to the web version of this article.)

where B is the bending stiffness and κ is the spontaneous curvature which models differential growth in the cross section. In the following, we will assume the bending stiffness to be constant. More refined models may account for changes in B due to lignification.

3.2. Growth law and time-evolution of the spontaneous curvature

In the present rod model, the active response of the plant is described by appropriate evolution laws for the stretch λ and for the spontaneous curvature κ . As for the stretch, we assume that cells extension occurs only in the growth zone of constant length $\ell_0 := \ell(0)$, where, following Bastien et al. (2014), we prescribe a constant elongation rate, i.e.,

$$\dot{\lambda} = \begin{cases} 0 & \text{if } 0 \leq s(S_0, t) < \ell(t) - \ell_0, \\ \frac{1}{\tau_g} & \text{if } s(S_0, t) \geq \ell(t) - \ell_0, \end{cases} \quad (19)$$

where τ_g is the characteristic time of growth induced by cell elongation and a superimposed dot denotes differentiation with respect to time.

Two main ingredients have been identified by Bastien et al. (2014) to model tropic movements of plants: (i) *graviception*, that aims to reorient the stem along the vertical, and (ii) *proprioception*, which tends to reduce the curvature of the organ. Both mechanisms determine the time evolution of the spontaneous curvature, such that, in the growth zone, its material time-derivative reads

$$\frac{d}{dt} \kappa(s(S_0, t), t) = G(s(S_0, t), t) + P(s(S_0, t), t), \quad (20)$$

where $G(s, t)$ and $P(s, t)$ are the gravitropic and proprioception signals.

From a biological standpoint, the response of the growth zone to gravi-stimulation is the result of several processes at the cellular level which are not yet completely understood. In particular, differential growth across the plant section is attributed to an auxin asymmetry between the upper and the lower part of the organ, and auxin redistribution is triggered by the sedimentation of statoliths in specialized cells called statocytes. Following Chauvet et al. (2019), we model this dynamics as

a viscous relaxation governed by the equation

$$\frac{d}{dt} \theta^s(s(S_0, t), t) = \frac{1}{\tau_a} \sin(\theta^s(s(S_0, t), t) - \theta(s(S_0, t), t)), \quad (21)$$

where τ_a is the characteristic duration of the statoliths avalanches and $\theta^s(s, t)$ is the local orientation of statoliths with respect to the vertical. Moreover, the same authors included in the model terms accounting for delay and memory processes that characterize the gravitropic signalling pathway. To model such processes, they proposed the following integral law

$$G(s, t) = -\frac{\beta}{R\tau_m\tau_g} \int_{-\infty}^{t-\tau_r} e^{-\frac{1}{\tau_m}(t-\tau_r-\tau)} \sin \theta^s(s, \tau) d\tau, \quad (22)$$

where τ_m is the memory time, τ_r is the reaction time or delay, β is a dimensionless gravitropic sensitivity, whereas R is the radius of the shoot's cross section.

In addition to the gravitropic response, it has been shown that, after a first phase where the organ responds to environmental stimuli, an independent mechanism takes place that hampers bending and favours a straight posture. The microscopic functioning of this phenomenon, called autotropism or autostraightening, is mostly unknown (Okamoto et al., 2015). However, we model it as proprioception following Bastien et al. (2013), such that

$$P(s, t) = -\frac{\gamma}{\tau_g} \theta'(s, t), \quad (23)$$

where γ is a dimensionless proprioception sensitivity.

3.3. A reduced model for the study of circumnutations: The regime $\tau_a \ll \tau_c \ll \tau_g$

As discussed in the previous section, four different time-scales control the evolution of growth-driven stretch and spontaneous curvature, i.e., τ_g , τ_a , τ_m and τ_r . Chauvet et al. (2019) determined the order of magnitudes of these characteristic times for wheat (*Triticum aestivum*) coleoptiles as follows: $\tau_a \approx 2$ min, $\tau_m \approx \tau_r \approx 12$ min, and $\tau_g \approx 1200$ min.

Since the period τ_c of most circumnutational oscillations is in the range of 20 – 300 min (Brown, 1993), we can assume that the statolith avalanche dynamics is much faster compared to circumnutations which, in turn, are much faster than the dynamics of cell elongation. On the one hand, the assumption of $\tau_g \gg \tau_c$ implies that we can neglect changes in length ℓ and bending stiffness B . Indeed, at short times compared to τ_g , the organ length approximately coincides with $\ell(0)$, and there is no distinction between current and reference arc-lengths. On the other hand, the condition $\tau_a \ll \tau_c$ yields $\theta^s(s, t) \approx \theta(s, t)$. Moreover, we neglect the proprioceptive term in the evolution law (20) since curvatures are relatively small, as confirmed by the results presented in the following. Based on these assumptions, we arrive at the reduced model

$$B[\theta''(s, t) - \kappa'(s, t)] = -q(\ell - s) \sin \theta(s, t), \quad \dot{\kappa}(s, t) = -\frac{\beta}{R\tau_m\tau_g} \int_{-\infty}^{t-\tau_r} e^{-\frac{1}{\tau_m}(t-\tau_r-\tau)} \sin \theta(s, \tau) d\tau \quad (24)$$

in the variables (θ, κ) for $s \in (0, \ell)$ and $t > 0$. Specifically, (24)₁ was obtained by first solving for the balance of forces (17)₁ in the absence of apical loads and then plugging the expression for the contact force in (17)₂, while accounting for the constitutive law of (18). As for (24)₂, it trivially follows from (20) with $P = 0$ and with the gravitropic signal given by (22), where θ replaces θ^s . The system of Eq. (24) is supplemented by the following boundary and initial conditions, namely

$$\theta(0, t) = 0, \quad \theta'(\ell, t) - \kappa(\ell, t) = 0, \quad (25)$$

holding $\forall t > 0$ as the basal end is clamped and the apical end is torque free, and

$$\theta(s, t) = \theta_0(s, t), \quad \kappa(s, 0) = \kappa_0(s), \quad (26)$$

prescribing respectively the past history of the angular coordinate and the initial datum for the spontaneous curvature evolution $\forall s \in [0, \ell]$.

Assuming sufficient regularity, we can combine the time-derivative of (24)₁ with the space-derivative of (24)₂, so that by a further differentiation with respect to time we arrive at

$$\ddot{\theta}'' + \frac{1}{\tau_m} \dot{\theta}'' + \frac{q(\ell - s)}{B} \left[\left(\ddot{\theta} + \frac{1}{\tau_m} \dot{\theta} \right) \cos \theta - \dot{\theta}^2 \sin \theta \right] + \frac{\beta}{R\tau_m\tau_g} \theta'(s, t - \tau_r) \cos \theta(s, t - \tau_r) = 0, \quad (27)$$

along with the boundary condition (25)₁ and

$$\ddot{\theta}'(\ell, t) + \frac{1}{\tau_m} \dot{\theta}'(\ell, t) + \frac{\beta}{R\tau_m\tau_g} \sin \theta(\ell, t - \tau_r) = 0, \quad (28)$$

holding $\forall t > 0$ and resulting from time differentiation of (25)₂.

4. Analysis of circumnutations in plant shoots

Guided by the study performed on the gravitropic spring-pendulum system, we proceed by first carrying out an analysis of the linearized version of Eq. (27). Such an analysis reveals the existence of periodic solutions that are reminiscent of circumnutations. Next, we introduce a computational model for the nonlinear governing equations that allows to explore the dynamics of model shoots in the oscillatory regime, providing evidence of a limit cycle associated with a Hopf bifurcation.

4.1. Linearization about the straight equilibrium configuration

By linearizing problem (27) and (28) about the equilibrium solution $\theta(s, t) \equiv 0$, we get the following fourth order partial differential equation with discrete delay

$$\ddot{\theta}''(s, t) + \frac{1}{\tau_m} \dot{\theta}''(s, t) + \frac{q(\ell - s)}{B} \left(\ddot{\theta}(s, t) + \frac{1}{\tau_m} \dot{\theta}(s, t) \right) + \frac{\beta}{R\tau_m\tau_g} \theta'(s, t - \tau_r) = 0, \tag{29}$$

supplemented by the boundary condition (25)₁ and

$$\ddot{\theta}'(\ell, t) + \frac{1}{\tau_m} \dot{\theta}'(\ell, t) + \frac{\beta}{R\tau_m\tau_g} \theta(\ell, t - \tau_r) = 0, \tag{30}$$

holding $\forall t > 0$ and resulting from the linearization of (28). Upon introducing four dimensionless parameters, i.e.,

$$y := \frac{q\ell^3}{B}, \quad \eta := \frac{\tau_r}{\tau_m}, \quad \sigma := \beta \frac{\tau_r^2}{\tau_g\tau_m}, \quad \mu := \frac{\ell}{R}, \tag{31}$$

Eq. (29) can be recast in dimensionless form as

$$\ddot{\theta}''(\hat{s}, \hat{t}) + \eta \dot{\theta}''(\hat{s}, \hat{t}) + y(1 - \hat{s}) \left(\ddot{\theta}(\hat{s}, \hat{t}) + \eta \dot{\theta}(\hat{s}, \hat{t}) \right) + \sigma \mu \hat{\theta}'(\hat{s}, \hat{t} - 1) = 0. \tag{32}$$

Here, $\hat{\theta}(\hat{s}, \hat{t}) := \theta(\hat{s}\ell, \hat{t}\tau_r)$ and primes and dots denote differentiation with respect to $\hat{t} := t/\tau_r$ and $\hat{s} := s/\ell$, respectively. As for the boundary conditions, we write

$$\hat{\theta}(0, \hat{t}) = 0, \quad \ddot{\theta}'(1, \hat{t}) + \eta \dot{\theta}'(1, \hat{t}) + \sigma \mu \hat{\theta}(1, \hat{t} - 1) = 0, \tag{33}$$

holding $\forall \hat{t} > 0$, whereas the initial condition is

$$\hat{\theta}(\hat{s}, \hat{t}) = \hat{\theta}_0(\hat{s}, \hat{t}), \tag{34}$$

which applies $\forall \hat{s} \in [0, 1], \forall \hat{t} \in [-1, 0]$.

We proceed with our analysis in the linear regime by seeking time-harmonic solutions of the form $\hat{\theta}(\hat{s}, \hat{t}) = \varphi(\hat{s})e^{\hat{\omega}\hat{t}}$ to (32)–(34). By substituting the form above in (32) we obtain

$$\varphi''(\hat{s}) + c\varphi'(\hat{s}) + y(1 - \hat{s})\varphi(\hat{s}) = 0, \tag{35}$$

where $c := \sigma \mu e^{-\hat{\omega}} / (\hat{\omega}^2 + \eta \hat{\omega})$. Integration of (35) leads to

$$\varphi(\hat{s}) = e^{-c\hat{s}/2} \left[c_1 \text{Ai}(x(\hat{s})) + c_2 \text{Bi}(x(\hat{s})) \right], \tag{36}$$

in which c_1 and c_2 are constants of integration, whereas $\text{Ai}(x)$ and $\text{Bi}(x)$ are the Airy functions of the first and second kind, respectively, and $x(\hat{s}) := [c^2/4 - y(1 - \hat{s})]/y^{2/3}$. By imposing the boundary conditions (33), and neglecting the trivial case of $c_1 = c_2 = 0$, we derive

$$\text{Ai}(x_0) \left(c \text{Ai}(x_1) + 2\sqrt[3]{y} \text{Bi}'(x_1) \right) - \text{Bi}(x_0) \left(c \text{Ai}(x_1) + 2\sqrt[3]{y} \text{Ai}'(x_1) \right) = 0, \tag{37}$$

where $x_0 := x(0), x_1 := x(1)$, and a prime denotes differentiation of the Airy functions with respect to their argument.

We numerically computed the roots of the characteristic Eq. (37) to explore the stability of model shoots of increasing length ℓ . To this aim, we exploited the FindRoot functionality of Mathematica v11.3.0.0. In agreement with Chelakkot and Mahadevan (2017) and Chauvet et al. (2019), we calibrated the model by setting $\beta = 0.8, \tau_g = 1200 \text{ min}, \tau_m = \tau_r = 12 \text{ min}, R = 0.5 \text{ mm}, E = 10^7 \text{ Pa}$ for the Young's modulus, and $q = \rho g A$ where $\rho = 10^3 \text{ Kg m}^{-3}$ is the mass density, A the cross-sectional area, and g the gravitational acceleration. For such a choice of model parameters, we determined values of the circular frequency $\hat{\omega}$ letting ℓ range in $[0, \ell_c]$. Here, ℓ_c denotes the critical length at which an elastic rod of bending stiffness B subject to a distributed, vertical load of magnitude q loses stability, that is

$$\ell_c := \sqrt[3]{\alpha B/q}, \tag{38}$$

with $\alpha \approx 7.837$, see Greenhill (1881).

We report in Fig. 3b the real (solid lines) and the imaginary (dashed lines) part of two roots of (37). As for the case of the gravitropic pendulum, we distinguish in the figure three regions corresponding to different dynamical responses of $\hat{\theta}(\hat{s}, \hat{t})$: (i) an exponential decay (light blue region, where roots are real and negative), (ii) a damped oscillation (orange region, where roots are complex conjugate with negative real part), and (iii) an increasing oscillation (green region, where roots are complex conjugate with positive real part) for $\ell > \ell^* \approx 0.895 \ell_c$.

Our analysis is restricted to solutions of the form introduced above, where spatial and temporal variables are separated. However, the presented results clearly indicate that the rod model suffers an instability in the linear regime as the shoot's length exceeds the critical value ℓ^* . This behaviour shares similarities with that exhibited by the gravitropic spring-pendulum system of the previous section. We shall next explore the dynamical response of the active rod model in the nonlinear regime by means of numerical computations.

4.2. Numerical implementation of the rod model

In this section, we introduce a numerical implementation of the nonlinear problem (24)–(26) in order to explore the regime of large amplitude oscillations exhibited by model shoots. Specifically, we solve Eq. (24) along with boundary conditions (25) and initial conditions (26) by using the finite element method.

As a first step towards the numerical formulation, it is convenient to introduce the auxiliary field $w(s, t)$ representing the delay integral, i.e.,

$$w(s, t) := \int_{-\infty}^{t-\tau_r} e^{-\frac{1}{\tau_m}(t-\tau_r-\tau)} \sin \theta(s, \tau) d\tau, \quad (39)$$

so that such integral may be computed from the solution of the differential equation

$$\dot{w}(s, t) = -\frac{1}{\tau_m} w(s, t) + \sin \theta(s, t - \tau_r). \quad (40)$$

With the definition (39), the Eq. (24)₂ for the evolution of the spontaneous curvature reads

$$\dot{\kappa}(s, t) = -\frac{\beta}{R\tau_m\tau_g} w(s, t). \quad (41)$$

To obtain the weak formulation of the governing equations, we multiply (24)₁, (40), and (41) by the test functions $\tilde{\theta}$, \tilde{w} , and $\tilde{\kappa}$, respectively, such that an integration in space along the interval $[0, \ell]$ leads to

$$\int_0^\ell (B(\theta'(s, t) - \kappa(s, t))\tilde{\theta}'(s, t) + q(\ell - s) \sin \theta(s, t)\tilde{\theta}(s, t)) ds = 0, \quad (42a)$$

$$\int_0^\ell (\dot{w}(s, t) + \frac{1}{\tau_m} w(s, t) + \sin \theta(s, t - \tau_r))\tilde{w}(s, t) ds = 0, \quad (42b)$$

$$\int_0^\ell (\dot{\kappa}(s, t) + \frac{\beta}{R\tau_m\tau_g} w(s, t))\tilde{\kappa}(s, t) ds = 0. \quad (42c)$$

In performing the integration by parts of the terms involving curvatures in (24)₁ we have accounted for the boundary condition (25)₂ and for the essential condition $\hat{\theta}(0, t) = 0$. Following standard finite element procedures, both the unknowns θ , w , κ and the corresponding test fields are discretized in space using linear Lagrange shape functions, while for the time discretization we choose the second-order generalized alpha method. The weak form equations were implemented and solved in COMSOL Multiphysics v5.4 using the Weak Form PDE mode.

Here, we focus our numerical study on the unstable regime predicted by the linear analysis of the previous section, see the green region of Fig. 3b. In particular, we choose a rod of length $\bar{\ell} := 0.91 \ell_c$ that is above the threshold ℓ^* . As the initial datum, we set

$$\theta_0(s, t) = a \operatorname{Re}(e^{\hat{\omega}t})\varphi(s/\bar{\ell}), \quad (43)$$

holding $\forall t \leq 0$. In the equation, a is the amplitude, $\hat{\omega}$ is the dimensional (complex) eigenvalue that solves (37) for $\ell = \bar{\ell}$, and $\varphi(s/\bar{\ell})$ is the corresponding eigenfunction as given by (36). Consequently, the initial condition for the delay integral w can be estimated from (39) under the hypothesis that $a \ll 1$, so that $\sin \theta_0(s, t) \approx \theta_0(s, t)$. To initialize the simulation with a zero-stress configuration, the magnitude of the distributed load is ramped from zero to q over a time interval much smaller than the fastest characteristic time scale of the system, i.e., τ_r , while the initial spontaneous curvature $\kappa(s, 0)$ equals the visible curvature $\theta'(s, 0)$ with $\theta(s, 0) = \theta_0(s, 0) = a\varphi(s/\bar{\ell})$.

Consistently with the theoretical results exposed in Section 4.1, our computational study reveals the onset of a limit cycle as the rod's length exceeds ℓ^* (≈ 7.1 cm, for the chosen parameters). In particular, we report in Fig. 3c several configurations of the rod at different times, clearly showing a symmetric oscillation with respect to the vertical line as the time spans half a period of the limit cycle (≈ 88 min, for a full cycle). In addition, Fig. 3d depicts the transverse displacement and the phase portraits related to the angle and position of the tip as functions of time. These show the signature of the limit cycle and provide a quantitative description of the dynamics of the system during its evolution towards the steady, oscillatory regime.

5. Conclusions and outlook

Inspired by the fascinating phenomenon of circumnutations, we investigated the effect of elastic deformations induced by gravity loading on the active response of plant shoots, an aspect that has been so far disregarded. To this aim, we first introduced a simple prototypical model, the so-called gravitropic spring-pendulum system. This was shown to be capable of capturing the main features of plants response to gravity. The simplicity of the model allowed us to perform a rigorous mathematical analysis to prove that a Hopf bifurcation occurs for a critical length of the pendulum.

To account for the complex nature of the interplay between elasticity and growth in plant shoots, we then derived a planar rod model built upon recent advances in the understanding of gravitropism. For this model, in a linearized setting, we proved the existence of oscillatory and diverging solutions above a critical length of the rod.

Finite element simulations allowed us to extend the analysis of the dynamics of model shoots into the nonlinear regime, with computational results confirming our theoretical findings. For a choice of material parameters consistent with the available literature on plant shoots, we found that rods of sufficient length may exhibit lateral oscillations of increasing amplitude, which eventually converge to limit cycles. This behavior strongly suggests the occurrence of a Hopf bifurcation, just as for the gravitropic spring-pendulum system, and is closely reminiscent of the periodic movements reported for elongating plant organs.

The present study supports the idea that plant nutations might be the result of a posture feedback control based on delayed graviresponses of a slender structure approaching the buckling critical length. This does not exclude that, in other circumstances such as in the case of climbing plants reaching for support, or in the coiling of tendrils, periodic helical motion may be the outcome of endogenous biological processes, leading to evolutionary advantages. In the case we consider, however, nutations may be simply a by-product of gravitropism -the attempt of plants to keep a vertical posture- and of deflections due to gravity loading. Here gravity plays two distinct roles that should not be confused. On the one hand, gravity causes the dynamics of statoliths and hence triggers the plant gravitropic response; on the other hand, the presence of gravity implies a load that the plant carries, with the corresponding elastic deflections, and this study shows that this effect is not negligible. Such a distinction must be kept in mind when altering the effect of gravity by means of experiments in Space or on Earth. Interestingly, the main features of our self-sustained oscillations depend on several distinct physical parameters, and this might explain the diversity of nutations observed in nature, even though each case should be carefully examined to rule out different biological mechanisms that our model has not yet taken into account. A general conclusion emerging from our analysis, that is worth emphasizing, is that the energy needed to sustain spontaneous oscillations is continuously supplied to the system by the internal biochemical machinery presiding the capability of plants to maintain a vertical pose.

We are aware of the inherent limitations of the proposed mechanical models, which are simplistic in many respects. Nevertheless, our quantitative results seem to be in good agreement with observations on circumnutations in the sense that both the critical length and the period of oscillations have the expected order of magnitude. Future work will include a quantitative assessment of the accuracy of the theoretical predictions in comparison with experimental observations. Moreover, the nonlinear rod model will be extended to account for a full three-dimensional description of the kinematics of plant nutations as recently developed by Bastien and Meroz (2016).

Beside their relevance in a biological context, studies on circumnutational movements in plants are providing inspiration for innovative designs in robotic applications from which, in turn, they benefit getting new insights. For instance, Del Dottore et al. (2018) have shown that soil penetration strategies mimicking circumnutations of plant roots may be advantageous when compared to more standard drilling techniques in the context of robotic soil exploration tasks.

Acknowledgments

ADS, DA, AL and GN acknowledge the support of the European Research Council (AdG-340685-MicroMotility). Part of this research was conducted while ADS was visiting the University of Cambridge, as a Visiting Scholar at Pembroke College, and as a visitor to the Newton Institute of Mathematical Sciences. The authors would like to congratulate Prof. Davide Bigoni on the occasion of his 60th birthday.

Appendix A. Hopf bifurcation: Existence of periodic solutions

In this section, we prove the supercritical Hopf bifurcation result for the gravitropic spring-pendulum system (6) stated in Section 2. To this end, we first recall some mathematical notions and results.

Definition A.1 (RFDE or DDE). Let $C := C([-d, 0], \mathbb{R}^n)$ for $d \in [0, \infty)$ and denote the norm of an element ϕ in C by $|\phi| := \sup_{\delta \in [-d, 0]} |\phi(\delta)|$. If $\mathbf{x} \in C([t_0 - d, t_1], \mathbb{R}^n)$ for $t_1 > t_0$ in \mathbb{R} , then for any $t \in [t_0, t_1]$, we define $\mathbf{x}_t \in C$ by

$$\mathbf{x}_t(\delta) := \mathbf{x}(t + \delta) \quad \forall \delta \in [-d, 0].$$

Given $D \subset \mathbb{R} \times C$ and $\mathbf{f} : D \rightarrow \mathbb{R}^n$, we say that the relation

$$\dot{\mathbf{x}}(t) = \mathbf{f}(t, \mathbf{x}_t) \tag{A.1}$$

is a *Retarded Functional Differential Equation* (RFDE), or a *Delay Differential Equation* (DDE), on D . A function $\mathbf{x} \in C([t_0 - d, t_1], \mathbb{R}^n)$ is said to be a *solution of (A.1) with initial value $\phi \in C$ at t_0* if $(t, \mathbf{x}_t) \in D$ for all $t \in [t_0, t_1]$, $\mathbf{x}_{t_0} \equiv \phi$ and $\mathbf{x}(t)$ has a continuous derivative on (t_0, t_1) , a right hand derivative at t_0 and satisfies (A.1) on $[t_0 - d, t_1)$. Such a solution will be denoted by $\mathbf{x}(t; \phi)$. Moreover, we say that Eq. (A.1) is

- (i) *linear* if $\mathbf{f}(t, \phi) = \mathbf{L}(t)\phi + \mathbf{h}(t)$, where $\mathbf{L}(t)$ is linear;
- (ii) *autonomous* if $\mathbf{f}(t, \phi) = \mathbf{g}(\phi)$ where \mathbf{g} does not depend on t .

Definition A.2 (Stability of equilibria). Let \mathbf{x}^* be an *equilibrium point* of $\dot{\mathbf{x}}(t) = \mathbf{f}(\mathbf{x}_t)$, i.e., $\mathbf{f}(\mathbf{x}^*) \equiv \mathbf{0}$. Then, the point \mathbf{x}^* is said to be

- (i) *stable* if, for any $\epsilon > 0$, there is $\delta > 0$ such that for any $\phi \in C$ with $|\phi| < \delta$, we have $|\mathbf{x}(t; \phi)| < \epsilon$ for $t \geq t_0 - d$;

- (ii) *unstable* if it is not stable;
- (iii) *asymptotically stable* if it is stable and there is $b > 0$ such that $|\phi| < b$ implies that $\|\mathbf{x}(t; \phi)\| \rightarrow \mathbf{x}^*$ as $t \rightarrow \infty$;
- (iv) a *local attractor* if there is a neighborhood U of \mathbf{x}^* such that $\lim_{t \rightarrow \infty} \text{dist}(\mathbf{x}(t; U), \mathbf{x}^*) = 0$, i.e., \mathbf{x}^* attracts elements in U uniformly.

Definition A.3 (Characteristic equation). Let $\mathbf{L} : \mathcal{C} \rightarrow \mathbb{R}^n$ be a continuous linear functional. We define the characteristic equation of the linear retarded equation $\dot{\mathbf{x}}(t) = \mathbf{L}(\mathbf{x}_t)$ as

$$\det(\omega \mathbf{I} - \mathbf{L}_\omega) = 0, \tag{A.2}$$

where $\mathbf{L}_\omega := [\mathbf{L}(\exp_\omega \mathbf{e}_1)] \dots [\mathbf{L}(\exp_\omega \mathbf{e}_n)]$. Here, $\exp_\omega(\delta) := e^{\omega\delta}$ and $\{\mathbf{e}_i\}_i$ is the canonical basis for \mathbb{R}^n .

Many well known results for ODEs can be shown to be still valid for RFDEs. In particular, if the characteristic equation of a linear system has a root with positive real part, then the origin is unstable. For asymptotic stability, it is necessary and sufficient to have each root ω with negative real part. If the RFDE is nonlinear and $\mathbf{0}$ is an equilibrium with all the characteristic roots (resp. a characteristic root) of the linearization at $\mathbf{0}$, having negative (resp. positive) real part, then classical approaches can be used to show that $\mathbf{0}$ is asymptotically stable (resp. unstable) for the nonlinear equation. Also the standard Hopf bifurcation theorem is valid for RFDEs in the following form.

Theorem A.1 (Hopf bifurcation). Consider a one-parameter family of autonomous RFDEs of the form

$$\dot{\mathbf{x}}(t) = \mathbf{F}(\mu, \mathbf{x}_t), \tag{A.3}$$

where $\mathbf{F} \in C^2(\mathbb{R} \times \mathcal{C}, \mathbb{R}^n)$ such that $\mathbf{0}$ is an equilibrium point of (A.3) for all μ . Define $L : \mathbb{R} \times \mathcal{C} \rightarrow \mathbb{R}^n$ by

$$L(\mu)\phi = D_\phi \mathbf{F}(\mu, \mathbf{0})\phi, \tag{A.4}$$

where $D_\phi \mathbf{F}(\mu, \mathbf{0})$ is the derivative of $\mathbf{F}(\mu, \phi)$ with respect to ϕ at $\phi = \mathbf{0}$. Assume that:

- (i) the linear equation $\dot{\mathbf{x}}(t) = L(\mathbf{0})\mathbf{x}_t$ has a pair of simple imaginary characteristic roots $\omega_0^\pm = \pm i\beta_0 \neq 0$ and all other characteristic roots $\omega_j \neq m\omega_0^+$ for any $m \in \mathbb{Z}$.

Then there is a $\mu_0 > 0$ and a simple characteristic root $\omega(\mu) = \alpha(\mu) + i\beta(\mu)$ of equation $\dot{\mathbf{x}}(t) = L(\mu)\mathbf{x}_t$ s.t. $\omega(0) = \omega_0^+$ and for $|\mu| < \mu_0$ it is continuously differentiable. Suppose that:

- (ii) $\text{Re}(\omega'(0)) = \alpha'(0) \neq 0$, where prime denotes differentiation with respect to μ .

Then, for μ close to zero, (A.3) has nontrivial periodic solutions, with period close to $2\pi/\beta_0$.

The linearization of (6) in the main text is a second order linear autonomous RFDE with discrete delay of the form

$$\ddot{y}(t) + a\dot{y}(t) + by(t-1) = 0, \tag{A.5}$$

which can be restated in system form as

$$\begin{cases} \dot{x}_1(t) = x_2(t) \\ \dot{x}_2(t) = -ax_2(t) - bx_1(t-1) \end{cases}$$

i.e.,

$$\dot{\mathbf{x}}(t) = \begin{bmatrix} 0 & 1 \\ 0 & -a \end{bmatrix} \mathbf{x}_t(0) + \begin{bmatrix} 0 & 0 \\ -b & 0 \end{bmatrix} \mathbf{x}_t(-1) =: L(a)\mathbf{x}_t.$$

Since the characteristic equation of (A.5) is equivalent to

$$\Delta(\omega) := (\omega^2 + a\omega)e^\omega + b = 0,$$

we are interested in determining the behaviour of its roots in terms of the parameter a . To this purpose, we restate the following result shown by Somolinos (1978).

Lemma A.1. Consider the equation

$$(\omega^2 + a\omega)e^\omega + b = 0 \tag{A.6}$$

for $b > 0$ and let ξ_b be the unique solution of $\xi^2 = b \cos(\xi)$ in $(0, \pi/2)$ and let $a_b := \sin(\xi_b)b/\xi_b$. Then the following holds for equation (A.6):

- (i) all roots have negative real parts if and only if $a > a_b$;
- (ii) for $a = a_b$, $\pm i\xi_b$ is the only pair of simple imaginary roots. In particular, no other root is an integer multiple of $i\xi_b$;
- (iii) there is an $\epsilon > 0$ and a root $\omega(a)$ that is continuously differentiable in $(a_b - \epsilon, a_b + \epsilon)$ s.t. $\omega(a_b) = i\xi_b$ and $\text{Re}(\omega'(a_b)) < 0$;
- (iv) for each $a < a_b$, there are precisely two roots ω with $\text{Re}(\omega) > 0$ and $\text{Im}(\omega) \in (-\pi, \pi)$.

The proof of Lemma A.1 uses the same argument applied by Hale and Lunel (1993) (see Theorem A.6 therein) which is based on the Pontryagin's method. Thanks to this result, one can prove the following theorem.

Theorem A.2. Consider $\mathbf{F} \in C^2(\mathbb{R} \times C([-1, 0], \mathbb{R}^2), \mathbb{R}^2)$,

$$\mathbf{F}(a, \mathbf{x}_t) = L(a)\mathbf{x}_t + \mathbf{f}(a, \mathbf{x}_t),$$

where $\mathbf{f}(a, \mathbf{0}) \equiv \mathbf{0}$ for all $a \in \mathbb{R}$ and $L(a) : C([-1, 0], \mathbb{R}^2) \rightarrow \mathbb{R}^2$ is the linear operator

$$L(a)\boldsymbol{\phi} := \begin{bmatrix} 0 & 1 \\ 0 & -a \end{bmatrix} \boldsymbol{\phi}(0) + \begin{bmatrix} 0 & 0 \\ -b & 0 \end{bmatrix} \boldsymbol{\phi}(-1),$$

where $b > 0$. Then the system $\dot{\mathbf{x}}(t) = \mathbf{F}(a, \mathbf{x}_t)$ undergoes a subcritical Hopf bifurcation at $a = a_b := \sin(\xi_b)b/\xi_b$ where ξ_b is the unique solution of $\xi^2 = b \cos(\xi)$ in $(0, \pi/2)$.

Proof. By Lemma A.1, the system $\dot{\mathbf{x}}(t) = \mathbf{F}(a - a_b, \mathbf{x}_t)$ verifies all the hypothesis of Theorem A.1. Therefore there is a subcritical Hopf bifurcation at $a = a_b$. \square

Finally, we prove the supercritical Hopf bifurcation result as stated in Section 2.

Corollary A.2.1. For $q\ell^2 < 2B$ Eq. (6) has a supercritical Hopf bifurcation at

$$\frac{q\ell^2}{2B} = y^* := 1 - \frac{\beta\tau_r}{\tau_g} \frac{\sin \xi^*}{\xi^*}, \tag{A.7}$$

where ξ^* is the unique root of $\xi = \frac{\tau_r}{\tau_m} \cot \xi$ in $(0, \pi/2)$.

Proof. The linearization of (6) about 0 is given by (7) which can be written in the dimensionless form as (9), i.e.,

$$\ddot{\theta}(\hat{t}) + \eta \dot{\theta}(\hat{t}) + \frac{\sigma}{(1-y)} \theta(\hat{t} - 1) = 0,$$

where by hypothesis $y < 1$ (or $q\ell^2 < 2B$). Since its characteristic equation is equivalent to

$$(\hat{\omega}^2 + \eta \hat{\omega})e^{\hat{\omega}} + \frac{\sigma}{(1-y)} = 0,$$

Theorem A.2 implies that a Hopf bifurcation occurs at

$$\eta = \frac{\sigma}{(1-y)} \frac{\sin \xi^*}{\xi^*}, \quad \xi^* = \frac{\sigma}{(1-y)} \frac{\cos \xi^*}{\xi^*}, \tag{A.8}$$

where $\xi^* \in (0, \pi/2)$. Taking the ratio between (A.8)_b and (A.8)_a, we get

$$\xi^* = \eta \cot \xi^*,$$

and then (A.8)_a can be rewritten as

$$y = 1 - \frac{\sigma}{\eta} \frac{\sin \xi^*}{\xi^*},$$

which is exactly (A.7). Moreover, since the inequality

$$\eta < \frac{\sigma}{(1-y)} \frac{\sin \xi^*}{\xi^*}$$

corresponds to

$$y > 1 - \frac{\sigma}{\eta} \frac{\sin \xi^*}{\xi^*},$$

we conclude that the Hopf bifurcation is supercritical in terms of y . \square

Supplementary material

Supplementary material associated with this article can be found, in the online version, at doi:10.1016/j.jmps.2019.103702.

Please cite this article as: D. Agostinelli, A. Lucantonio and G. Noselli et al., Nutations in growing plant shoots: The role of elastic deformations due to gravity loading, Journal of the Mechanics and Physics of Solids, <https://doi.org/10.1016/j.jmps.2019.103702>

References

- Abe, K., Takahashi, H., Suge, H., 1996. Lazy gene (La) responsible for both an agravitropism of seedlings and lazy habit of tiller growth in rice (*oryza sativa* L.). *J. Plant Res.* 109, 381–386.
- Arnal, C., 1953. Recherches sur la nutation des coléoptiles. Librairie générale de l'enseignement.
- Badot, P., Melin, D., Garrec, J., et al., 1990. Circumnutation in *Phaseolus vulgaris*. II. potassium content in the free-moving part of the shoot. *Plant Physiol. Biochem. (Paris)* 28, 123–130.
- Bastien, R., Bohr, T., Mouliá, B., Douady, S., 2013. Unifying model of shoot gravitropism reveals proprioception as a central feature of posture control in plants. *Proc. Natl. Acad. Sci. USA* 110, 755–760.
- Bastien, R., Douady, S., Mouliá, B., 2014. A unifying modeling of plant shoot gravitropism with an explicit account of the effects of growth. *Front. Plant Sci.* 5, 136.
- Bastien, R., Meroz, Y., 2016. The kinematics of plant nutation reveals a simple relation between curvature and the orientation of differential growth. *PLoS Comput. Biol.* 12, e1005238. doi:10.1371/journal.pcbi.1005238.
- Bigoni, D., Kirillov, O.N., Misseroni, D., Noselli, G., Tommasini, M., 2018. Flutter and divergence instability in the pflüger column: experimental evidence of the Ziegler destabilization paradox. *J. Mech. Phys. Solids* 116, 99–116. doi:10.1016/j.jmps.2018.03.024.
- Bigoni, D., Noselli, G., 2011. Experimental evidence of flutter and divergence instabilities induced by dry friction. *J. Mech. Phys. Solids* 59, 2208–2226. doi:10.1016/j.jmps.2011.05.007.
- Brown, A.H., 1993. Circumnutations: from darwin to space flights. *Plant Physiol.* 101, 345.
- Brown, A.H., Chapman, D.K., 1984. Circumnutation observed without a significant gravitational force in spaceflight. *Science* 225, 230–232.
- Brown, A.H., Chapman, D.K., Lewis, R.F., Venditti, A.L., 1990. Circumnutations of sunflower hypocotyls in satellite orbit. *Plant Physiol.* 94, 233–238.
- Bünning, E., et al., 1953. *Entwicklungs- und bewegungsphysiologie der pflanze*. Springer.
- Chapman, D.K., Johnsson, A., Karlsson, C., Brown, A., Heathcote, D., 1994. Gravitropically-stimulated seedlings show autotropism in weightlessness. *Physiol. Plant* 90, 157–162.
- Chauvet, H., Mouliá, B., Legué, V., Forterre, Y., Pouliquen, O., 2019. Revealing the hierarchy of processes and time-scales that control the tropic response of shoots to Gravi-stimulations. *J. Exper. Botany* 70, 1955–1967.
- Chelakkot, R., Mahadevan, L., 2017. On the growth and form of shoots. *J. R. Soc. Interf.* 14, 20170001.
- Correll, M.J., Kiss, J.Z., 2008. Space-based Research on Plant Tropisms. In: Gilroy, S., Masson, P. (Eds.), *Plant Tropisms*. Blackwell Publishing, Oxford, pp. 161–182.
- Darwin, C., 1880. *The Power of Movement in Plants*. John Murray, London.
- Del Dottore, E., Mondini, A., Sadeghi, A., Mattoli, V., Mazzolai, B., 2018. An efficient soil penetration strategy for explorative robots inspired by plant root circumnutation movements. *Bioinsp. Biomimet.* 13, 015003.
- Dumais, J., 2013. Beyond the sine law of plant gravitropism. *Proc. Natl. Acad. Sci. USA* 110, 391–392.
- Gilroy, S., Masson, P., 2008. *Plant Tropisms*. Blackwell Publishing, Oxford.
- Gradmann, H., 1922. Die fünfphasenbewegung der ranken. *Jahrbücher für wissenschaftliche Botanik* 61, 169–204.
- Gradmann, H., 1926. Die bewegungen der ranken und die überkrümmungstheorie. *Jahrbücher für wissenschaftliche Botanik* 65, 224–278.
- Greenhill, A.G., 1881. Determination of the greatest height consistent with stability that a vertical pole or mast can be made, and of the greatest height to which a tree of given proportions can grow. *Proc. Camb. Philos. Soc.* 4, 65–73.
- Hale, J.K., Lunel, S.M.V., 1993. *Introduction to Functional Differential Equations*. Springer Science & Business Media.
- Hamant, O., Mouliá, B., 2016. How do plants read their own shapes? *New Phytol.* 212, 333–337.
- Hammer, L., Gessner, F., 1958. Lichtedinge wachstumsschwingungen bei *Helianthus annuus*. *Österreichische botanische Zeitschrift* 105, 529–549.
- Hatakeda, Y., Kamada, M., Goto, N., Fukaki, H., Tasaka, M., Suge, H., Takahashi, H., 2003. Gravitropic response plays an important role in the nutational movements of the shoots of *Pharbitis nil* and *Arabidopsis thaliana*. *Physiol. Plantarum* 118, 464–473.
- Heathcote, D.G., Aston, T., 1970. The physiology of plant nutation: i. nutation and geotropic response. *J. Exp. Bot.* 21, 997–1002.
- Israelsson, D., Johnsson, A., 1967. A theory for circumnutations in *Helianthus annuus*. *Physiol. Plant* 20, 957–976. doi:10.1111/j.1399-3054.1967.tb08383.x.
- Joerrens, G., 1957. *Nutationsbewegungen bei Triticum-Koleoptilen*. Ph.D. thesis
- Johnsson, A., Heathcote, D., 1973. Experimental evidence and models on circumnutations. *Zeitschrift für Pflanzenphysiologie* 70, 371–405. doi:10.1016/S0044-328X(73)80117-5.
- Johnsson, A., Jansen, C., Engelmann, W., Schuster, J., 1999. Circumnutations without gravity: a two-oscillator model. *J. Gravitat. Physiol.* 6, 9–12.
- Johnsson, A., Solheim, B.G.B., Iversen, T.H., 2009. Gravity amplifies and microgravity decreases circumnutations in *Arabidopsis thaliana* stems: results from a space experiment. *New Phytol.* 182, 621–629. doi:10.1111/j.1469-8137.2009.02777.x.
- Kim, H.-j., Kobayashi, A., Fujii, N., Miyazawa, Y., Takahashi, H., 2016. Gravitropic response and circumnutation in pea (*Pisum sativum*) seedling roots. *Physiol. Plant* 157, 108–118.
- Kiss, J.Z., 2006. Up, down, and all around: how plants sense and respond to environmental stimuli. *Proc. Natl. Acad. Sci. USA* 103, 829–830.
- Kiss, J.Z., 2009. Plants circling in outer space. *New Phytol.* 182, 555–557.
- Kitazawa, D., Hatakeda, Y., Kamada, M., Fujii, N., Miyazawa, Y., Hoshino, A., Iida, S., Fukaki, H., Morita, M.T., Tasaka, M., et al., 2005. Shoot circumnutation and winding movements require gravisensing cells. *Proc. Natl. Acad. Sci. USA* 102, 18742–18747.
- Kitazawa, D., Miyazawa, Y., Fujii, N., Nitasaka, E., Takahashi, H., 2008. Characterization of a novel gravitropic mutant of morning glory, *weeping2*. *Adv. Space Res.* 42, 1050–1059.
- Kobayashi, A., Kim, H.-j., Tomita, Y., Miyazawa, Y., Fujii, N., Yano, S., Yamazaki, C., Kamada, M., Kasahara, H., Miyabayashi, S., Shimazu, T., Fusejima, Y., Takahashi, H., 2019. Circumnutation movement in rice coleoptiles involves the gravitropic response: analysis of an agravitropic mutant and space-grown seedlings. *Physiol. Plant* 165, 464–475. doi:10.1111/pp1.12824.
- Meroz, Y., Bastien, R., Mahadevan, L., 2019. Spatio-temporal integration in plant Tropisms. *J. R. Soc. Interf.* 16, 20190038.
- Millet, B., Melin, D., Badot, P.M., 1988. Circumnutation in *Phaseolus vulgaris*. i. growth, osmotic potential and cell ultrastructure in the free-moving part of the shoot. *Physiol. Plant* 72, 133–138.
- Millet, B., Melin, D., Bonnet, B., Ibrahim, C., Mercier, J., 1984. Rhythmic circumnutation movement of the shoots in *Phaseolus vulgaris* L. *Chronobiol. Int.* 1, 11–19.
- Mugnai, S., Azzarello, E., Masi, E., Pandolfi, C., Mancuso, S., 2015. Nutation in Plants. In: Mancuso, S., Shabala, S. (Eds.), *Rhythms in Plants*. Springer, pp. 19–34.
- Noll, F., 1885. Über rotierende nutation an etiolierten keimpflanzen. *Botanische Zeitung* 43, 664–670.
- Okamoto, K., Ueda, H., Shimada, T., Tamura, K., Kato, T., Tasaka, M., Morita, M.T., Hara-Nishimura, I., 2015. Regulation of organ straightening and plant posture by an actin-myosin XI cytoskeleton. *Nat. Plants* 1, 15031.
- Palm, L.H., 1827. Über das winden der pflanzen: Eine botanisch-physiologische abhandlung. Löfflund.
- Pouliquen, O., Forterre, Y., Bérut, A., Chauvet, H., Bizet, F., Legue, V., Mouliá, B., 2017. A new scenario for gravity detection in plants: the position sensor hypothesis. *Phys. Biol.* 14, 035005.
- Rawitscher, F., 1932. *Geotropismus der pflanzen*. G. Fischer, Jena.
- von Sachs, J., 1875. *Textbook of Botany, English Translation Edition*. Oxford University Press, Oxford.
- von Sachs, J., 1882. Über orthotrope und plagiotrope pflanzenheile. *Arbeiten des Botanischen Instituts in Würzburg* 2, 226–284.
- Schuster, J., 1996. Studying circumnutation of the hypocotyls of *Arabidopsis thaliana* and *Helianthus annuus*. Ph.D. thesis
- Shabala, S., 2003. Physiological Implications of Ultradian Oscillations in Plant Roots. In: Abe, J. (Ed.), *Roots: The Dynamic Interface between Plants and the Earth*. Springer, Dordrecht, pp. 217–226.

- Shabala, S.N., Newman, I.A., 1997. Proton and calcium flux oscillations in the elongation region correlate with root nutation. *Physiol. Plant* 100, 917–926.
- Somolinos, A.S., 1978. Periodic solutions of the sunflower equation: $\ddot{x} + (a/r)x + (b/r) \sin x(t - r) = 0$. *Q Top Q. Appl. Math.* 35, 465–478. doi:10.1090/qam/465265.
- Yoshihara, T., Iino, M., 2006. Circumnutation of rice coleoptiles: its relationships with gravitropism and absence in lazy mutants. *Plant, Cell Environ.* 29, 778–792.